Article

FACILE HYDROTHERMAL SYNTHESIS OF NIOBIUM PENTOXIDE SEMICONDUCTOR AND THEIR APPLICATION IN THE PHOTODEGRADATION OF DYES AND REDUCTION OF FREE FAT ACIDS IN WASTE OIL

Camilo Aurélio Brandão Crisóstomo[a], Fernanda Barbosa Damaceno[a], Luele Ribeiro de Sousa Barbosa[a], Jânio Santos Almeida[a], Walker Vinicius Ferreira do Carmo Batista[a], Andréa Renata Malagutti[b], João Paulo de Mesquita[c], Juliana Arriel Torres[d], Gustavo Duran Iga[d], Caue Ribeiro de Oliveira[d], Roberto Ananias Ribeiro[e] and Henrique A. J. L. Mourão[a,f,*]

[a]Programa de Pós-Graduação em Química (PPGQ), Universidade Federal dos Vales do Jequitinhonha e Mucuri (UFVJM), 39100-000 Diamantina – MG, Brasil

[b]Departamento de Farmácia (DEFAR), Universidade Federal dos Vales do Jequitinhonha e Mucuri (UFVJM), 39100-000 Diamantina – MG, Brasil

[c]Departamento de Química (DEQUI), Universidade Federal dos Vales do Jequitinhonha e Mucuri (UFVJM), 39100-000 Diamantina – MG, Brasil

[d]Embrapa Instrumentação, 13560-970 São Carlos – SP, Brasil

[e]Instituto Federal do Norte de Minas Gerais, Campus Salinas (IFNMG), 39560-000 Salinas – MG, Brasil

[f]Instituto de Ciência e Tecnologia (ICT), Universidade Federal dos Vales do Jequitinhonha e Mucuri (UFVJM), 39100-000 Diamantina – MG, Brasil

Received: 10/03/2023; accepted: 03/14/2024; published online: 05/29/2024

We report a facile hydrothermal method for the synthesis of niobium pentoxide (Nb_2O_5) under two different temperatures, 120 °C (Nb_2O_5-120) and 150 °C (Nb_2O_5-150). The obtained materials were characterized by structural, optical and morphological techniques. Also, the photocatalytic properties of the Nb_2O_5 samples were evaluated in two reactions under ultraviolet (UVC) irradiation: degradation of methylene blue (MB) and indigo carmine (IC) dyes; and esterification of free fatty acids (FFA) present in waste cooking oil (WCO). The Nb_2O_5 was formed at different temperatures of synthesis, and the increase in temperature did not cause significant changes in the structural and optical characteristics, but resulted in an increased surface area of the synthesized materials. Both synthesized materials showed excellent efficiency for dye photodegradation. The sample Nb_2O_5-150 presented the best performance for the MB photodegradation, with almost 85% of the removal efficiency. In this case, the adsorption of MB molecules on the surface of the material was high due to the favorable electrostatic interaction and also because of its high surface area. For the IC photodegradation, the adsorption was insignificant, and both samples presented approximately 100% of the removal efficiency. These materials were also promising for the reduction of free fat acids in waste oil by photoesterification.

Keywords: Nb_2O_5; hydrothermal method; photodegradation; photoesterification; UVC irradiation.

INTRODUCTION

Semiconductor materials have great potential for application in heterogeneous photocatalysis using sunlight or artificial light as an activation source.[1,2] Recently, heterogeneous photocatalysis has been studied, mainly in relation to its application in environmental remediation. Several studies have shown that it is possible to completely degrade organic contaminants such as phenols, hydrocarbons, insecticides, dyes, among others.[3-8] On the other hand, photocatalysis is a promising technological solution for the production of various synthetic precursors and products for fine chemicals, as well as for the production of biofuels.[9-17]

Niobium pentoxide (Nb_2O_5) is an important "n-type" semiconductor due to its excellent properties like non-toxicity, corrosion resistance, thermodynamic stability, high specific surface area, high selectivity and strength of surface acid sites. The high stability of Nb_2O_5 in aqueous media for various reactions acting as a solid acid catalyst, as well as its good abundance, make it an attractive photoactive material.[5-7,18-23] The band gap of Nb_2O_5 varies in the range of 3.1 to 4.0 eV, with a high absorption in the ultraviolet (UV) light region.[2,23,24] Nb_2O_5 has a high structural complexity due to its characteristic polymorphism, whose degree is related to the synthesis method and its variables, such as the nature of the precursors, processing time and temperature.[4,5,25] Hydrothermal treatments have a high potential to produce Nb_2O_5 structures with high photocatalytic activity, and they are carried out at low temperatures. This process allows the crystallization to occur under mild conditions and does not eliminate the hydroxyl groups formed on the surfaces. This results in a material with a high surface area and greater number of acid sites.[4,5,26]

Nb_2O_5 with different structures is promising for application in photocatalysis under UV[5,6] and visible[7,8] irradiation, such as in advanced oxidative processes (AOP's) and photodegradation of different organic dyes, such as methylene blue (MB);[5-7,27] indigo carmine (IC);[3] and methylene orange (MO).[8]

Some semiconductors have been used efficiently for the production of biodiesel from a wide range of low-cost feedstocks (such as WCO) using a two-step (photo) catalytic process. Firstly, the esterification of free fat acids (FFA) (present in oil) with alcohol is catalyzed by a photocatalyst under UV irradiation. Secondly, the transesterification of triglycerides (TG) with alcohol is catalyzed by NaOH or KOH.[12-17,28] As far as our knowledge goes, the photoesterification of FFA which are present in vegetable oils for biodiesel production has not already been reported using Nb_2O_5 as a heterogeneous photocatalyst.

In this paper, we describe the hydrothermal synthesis of Nb_2O_5 and its application in the photodegradation of dyes (methylene blue (MB) and indigo carmine (IC)) and the photoesterification of free fatty acids (FFA) present in waste cooking oil (WCO).

*e-mail: henrique.mourao@ict.ufvjm.edu.br

EXPERIMENTAL

Materials preparation

The Nb_2O_5 samples were obtained from hydrothermal synthesis using the precursor niobium ammonium oxalate ($NH_4[NbO(C_2O_4)_2(H_2O)_2].nH_2O$) which was donated by CBMM (Companhia Brasileira de Metalurgia e Mineração).[29] Firstly, 1.0 g of the precursor was solubilized into 80 mL of distilled water. After that, this mixture was placed into Teflon vessel heated in a stainless-steel autoclave at 120 or 150 °C for 5 h of hydrothermal treatment. The formed precipitate was wash with distilled water, centrifuged and dried to obtain the final powder. The prepared samples were referred as Nb_2O_5-120 and Nb_2O_5-150, respectively.

Materials characterization

The X-ray (powder) diffraction (XRD) analysis were obtained using a Shimadzu XRD-6000 diffractometer (Tokyo, Japan) with monochromatic CuKα radiation (λ = 0.15406 nm) using scanning speed of 2° min^{-1} in the 2θ range from 10 to 70°. Fourier transform infrared spectra (FTIR) were obtained from 400 to 4000 cm^{-1} using a Varian 640-IR FTIR spectrometer (São Paulo, Brazil) in ATR mode. The morphology was examined by scanning electron microscopy (SEM), using a Hitachi TM-3000 microscope (Tokyo, Japan) and the elemental composition was evaluated by energy dispersive spectroscopy (EDS) with the detector Oxford Swift ED 3000 (Tokyo, Japan). Diffuse reflectance spectrometry (DRS) analyses were performed with a UV-Vis Shimadzu UV-2600 spectrophotometer (Tokyo, Japan) in the range of 300-700 nm. The band gap energy was estimated by using the Tauc equation from the x-axis intercept of the tangent lines of each curve, as described in the previous study.[29] Zeta-potential analyses were performed on a Malvern® Zetasizer Nano instrument. For this, 1.0 mg of sample was suspended in 10 mL of deionized water and dispersed by sonication using a Branson Digital sonicator (Hampton, USA). Aqueous solutions of sodium hydroxide (NaOH, Synth, Diadema, Brazil) and hydrochloric acid (HCl, Synth, Diadema, Brazil) were used to adjust the pH of suspensions during analysis. The values of specific surface area (SSA) were estimated according to the Brunauer-Emmett-Teller (BET) method by using N_2 physisorption at 77 K data obtained in Micromeritics ASAP-2020 (Norcross, USA) equipment. The calculation was taken from the linear points of the isotherms at low pressure interval of $P\,P_0^{-1}$ from 0.01 to 0.05, as recommended in Rouqerol criteria. The pore diameter was obtained by Barrett-Joyner-Halenda (BJH) method from the desorption branch and the Harkins and Jura thickness curve with BJH standard correction. The total pore volume was calculated at the 0.95 $P\,P_0^{-1}$ with the single-point adsorption method.

Photocatalytic tests

Photodegradation of the methylene blue (MB) and indigo carmine (IC)

The photocatalytic tests with synthesized Nb_2O_5 samples were carried out using a photoreactor equipped with six UVC fluorescent lamps placed on the top of the photoreactor (distance of 0.24 m from the reaction mixture). The temperature was held constant by a thermostatically controlled water circulator that maintained the temperature at about 20 °C. Aqueous suspensions were obtained by dispersing 10 mg of photocatalyst in 20 mL of aqueous solutions of each dye (MB at 10 mg L^{-1} or IC at 30 mg L^{-1}). Before the photocatalytic tests, the suspensions were previously kept in the dark for 12 h to ensure the adsorption/desorption equilibrium between the catalyst and the dye molecules. The decrease in the concentration of the dye was analyzed in a Double Beam spectrophotometer (Shimadzu UV 6300 PC, Tokyo, Japan) at 664 nm for MB and 610 nm for IC. All measurements were performed in triplicate.

The residual solutions of MB and IC obtained after photodegradation test were also analyzed by high performance liquid chromatography (HPLC) on an Agilent Technologies-1200 instrument (Santa Clara, USA) equipped with a C18 column and with a UV-Vis detector using atmospheric pressure ionization. The detection wavelengths were 625, 508 and 427 nm, and the mobile phase used was water and methanol mixture (molar proportion of 25:75). The analysis conditions were: dilution of 2 µL of the sample in 20 mL of distilled water, injection of 15 µL, 10 min of running with a flow rate of 1.0 mL min^{-1} and temperature of 30 °C.

Photocatalytic esterification of WCO with ethanol

The waste cooking oil (WCO) was a mixture of different vegetable oils, provided by local restaurants. The WCO was collected, filtered, and stored in a hermetically sealed PVC (polyvinyl chloride) vessel for analysis and utilization in the tests. Absolute ethanol was of analytical grade (> 99%) and was purchased from Synth (Diadema, Brazil). The tests were performed at 40 °C under UVC irradiation for 1 h. The photocatalyst concentration was 1 wt.% of the initial WCO mass. The ethanol/oil molar ratios used were 20:1 and 5:1. These reaction conditions were based on previous studies.[12,13,17] A blank experiment was run without the catalyst under the same experimental conditions. After reactions, the mixture was transferred to the funnel, and it was left to stand to separate the two liquid phases. The lower oil layer was probably composed of ethyl esters, unreacted triglycerides, and the solid catalyst.[12,13] These samples were centrifuged to separate the catalyst from the solution. The supernatant was centrifuged for further acid value (AV) analysis. The upper layer was probably a mixture of ethanol and the water produced during the reaction.[12,13] The acid value (AV) of the initial WFO and after its use in tests was determined following the AOCS Cd-3d-63 method of American Oil Chemists Society (AOCS) by titrating the sample with a standard solution of NaOH (0.1 mol L^{-1}). The AV (mg KOH g^{-1}) was determined using the Equation 1:[12-14]

$$AV = \frac{V \times f \times C \times 56.11}{m} \quad (1)$$

where: V is the volume of NaOH (in mL) standard solution consumed to reach the titration end point; F is the NaOH solution correction factor; C is the concentration of NaOH standard solution (mol L^{-1}); 56.11 is the molecular weight of KOH (g mol^{-1}); m is the weight (g) of the test sample. The FFA conversion (C_{FFA}) during the esterification was determined using the Equation 2:[12-14]

$$\%C_{FFA} = \frac{AV_i - AV_f}{AV_i} \times 100 \quad (2)$$

where: AV_i is the initial acid value of the WCO and AV_f is the final acid value of the WCO after the FFA esterification reaction.

RESULTS AND DISCUSSION

Characterization of the Nb_2O_5 samples

Figure 1 shows the XRD patterns of the synthesized samples. Although the peak intensities were slightly different, the both samples showed similar diffractograms with broad diffractions peaks in 2θ equal to 22.8, 26.2, 34.7, 46.4 and 55.3°, indexed to the

crystallographic planes (001), (100), (111), (002) and (102) of the tetragonal phase of Nb_2O_5 (JCPDS number 18-0911), respectively.[30]

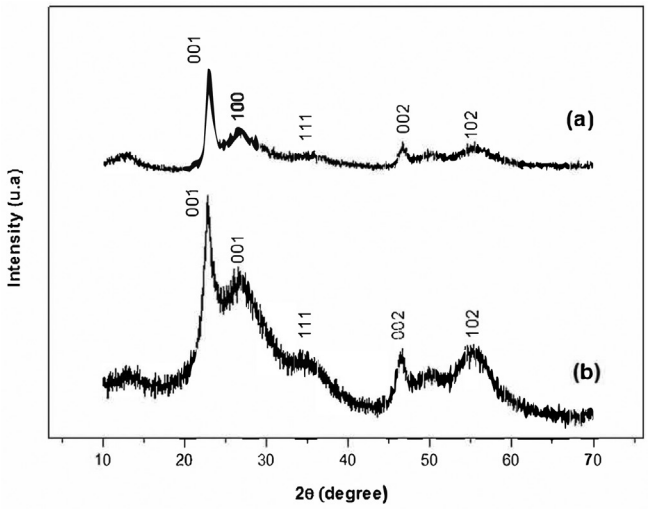

Figure 1. *XRD patterns of the samples: (a) Nb_2O_5-150; (b) Nb_2O_5-120 (ICSD 25750 - JCPDS number 18-0911)*

The broad peaks are relative to the hydrated niobium oxide because the appearance of the peak in the XRD at 2θ ≈ 26° is related to the intermediate conditions of crystallization.[4] These results are similar to those reported by other works[4,8,30-33] that used the hydrothermal method for Nb_2O_5 synthesis. Nb_2O_5 can have an amorphous structure or different crystalline structures depending on the method and variables of synthesis, such as time and temperature. Under hydrothermal conditions, at a moderate temperature, the pressure is high, favoring the solubility of the materials since the solvent remains liquid even above its normal vaporization point.[4,5,26,34] These conditions can influence several material characteristics, including morphology and crystalline phase, among others. Thus, it is possible to conclude that the hydrothermal treatment favored the beginning of the formation of the tetragonal phase under the studied conditions. Also, it is possible to observe that the temperature of the hydrothermal treatment did not significantly alter the crystalline structure of Nb_2O_5, since the two samples showed similar diffractograms.[4,8]

The FTIR spectra obtained are shown in Figure 2. For a better understanding, the spectra were divided into three main regions of bands, indicated by regions I to III in Figure 2.

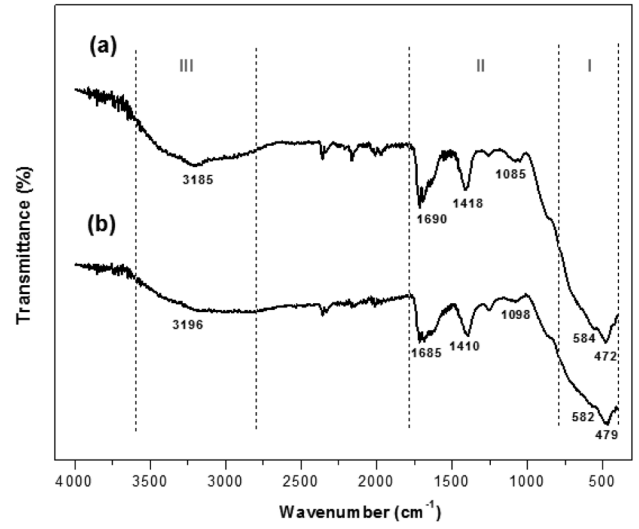

Figure 2. *FTIR spectra of the samples: (a) Nb_2O_5-150; (b) Nb_2O_5-120*

In region I, the band located at 584 cm^{-1} can be attributed to the ν(Nb–O–Nb) vibrations, and at 472 cm^{-1} can be attributed to the ν(Nb–O) vibration.[30,35] In region II, the band at 1690 cm^{-1} is due to the bending vibrations of H_2O molecules and also to the C=O bond; the bands around 1418 cm^{-1} are characteristic of N–H groups and organic compounds, corresponding to the residual organic component of the niobium precursor; and the band at 1085 cm^{-1} is related to the presence of carbon-nitrogen species and the vibration of the C–N bond.[8,30,35,36] A large absorption around the band at 3185 cm^{-1} (region III) is due to the stretching vibration of the –OH surface groups, adsorbed H_2O and the Nb–OH bond (surface hydroxylation).[4,30,35,37] The high intensity of the bands related to the surface –OH groups is directly related to the quantification of these groups in the samples, which act as Brønsted acid sites.[37,38] Assuming that the hydroxyl radical formation mechanism plays an important role in the photocatalytic process, it is worth pointing out that the number of acid groups on the surface (–OH, Nb=O and others) can have a positive effect on the photocatalytic activity of the Nb_2O_5 samples.[4]

The morphologies of the synthesized samples were analyzed by SEM (Figure 3).

The images showed that the synthesized samples are composed of aggregate, and the particles do not have well-defined morphology. Also, it is not possible to observe significant changes in the morphology between the two synthesized samples. Additionally, the elemental compositions of both samples obtained by EDS (Table 1) were very similar, and the values of the O/Nb molar ratios were very close to those of the expected stoichiometry of the Nb_2O_5 (2.5).

The optical absorption properties of the Nb_2O_5 samples were investigated through diffuse reflectance spectroscopy. Figure 4a presents the obtained UV-Vis (DRS) spectra of the synthesized Nb_2O_5 materials. According to the UV-Vis spectra shown in Figure 4a, the absorption edges of both Nb_2O_5 samples are approximately 380 nm, suggesting that the Nb_2O_5 samples are UV-responsive photocatalysts. The band gap energy values (Eg) were determined by using the Tauc plot for a direct transition semiconductor,[29] considering the x-axis intercept of the tangent lines (linear extrapolation), as shown in Figure 4b. The corresponding band gap values of the Nb_2O_5 samples are very similar (3.25 and 3.30 eV for Nb_2O_5-150 and Nb_2O_5-120, respectively), and they are in accordance with reported values in the literature of the Nb_2O_5 materials.[4,8,30-33] This high Eg value indicated that the Nb_2O_5 photocatalysts could not be activated by visible radiation, but they could be considered promising photocatalysts when irradiated with UV radiation.[7,8]

Additionally, Figure 1S (Supplementary Material) shows the zeta potential as a function of pH. These results demonstrate that both synthesized samples of Nb_2O_5 present a very low isoelectric point (IEP), and they are stable even under pH conditions higher than IEP.

In this way, comparing the structural and morphological data of the two synthesized samples, it can be affirmed that the Nb_2O_5 was formed even at the lowest temperature of synthesis.

Photocatalytic tests

Methylene blue (MB) and indigo carmine (IC) dyes photodegradation

The photoactivity of the synthesized Nb_2O_5 samples was first evaluated through the photodegradation of two different dyes: methylene blue (MB) and indigo carmine (IC). Firstly, it has been observed that there was a high adsorption of the MB molecules on the materials surface even in the dark before the photocatalytic test. This could be explained by the low IEP of the synthesized samples and by the cationic surface characteristics of the MB molecules, something

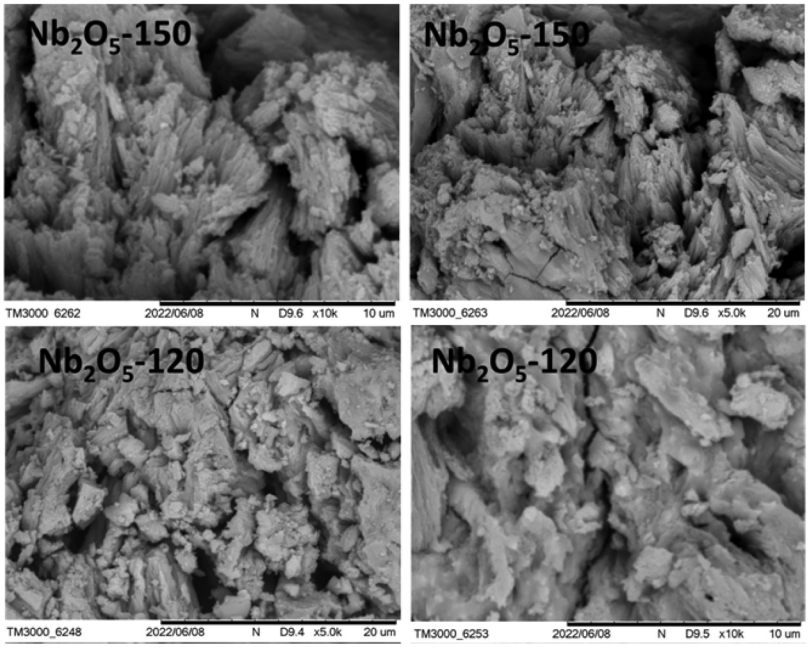

Figure 3. *SEM images of the Nb_2O_5 samples*

Table 1. Elemental composition (% mol) of the synthesized samples and O/Nb molar ratios obtained by EDS

Element	Nb_2O_5-120	Nb_2O_5-150
Oxygen	74%	72%
Niobium	26%	28%
O/Nb ratio	2.8	2.6

that is not the case with the IC molecules.[3,7,39] Figures 5a and 6a show the photocatalytic curves for the MB and IC photodegradation using as-synthesized Nb_2O_5 samples, respectively. Photodegradation curves were obtained by plotting the dye concentrations as a function of exposure time under UVC irradiation, where C_0 is the initial dye concentration and C is the dye concentration at a specific time (t). The rate constants (k) were estimated using the pseudo-first-order model, which proved to be very appropriate (high linear correlation) for the both dyes.[40] The fits are in Figures 5b (MB) and 6b (IC). Also, the values of k and the linear correlation coefficients (R^2) are presented in Table 2.

For the MB photodegradation (Figure 5a), the direct photolysis was negligible with a small reduction of about 5% even after 260 min under irradiation. Also, it was possible to observe a difference between the photodegradation efficiencies of the synthesized samples. The sample Nb_2O_5-150 ($k = 0.0067\ min^{-1}$ with almost 85% of removal efficiency) showed higher photoactivity than sample Nb_2O_5-120 ($k = 0.0038\ min^{-1}$) which presented approximately 60% of removal efficiency (Figure 2Sa, Supplementary Material). This result is probably related to the better interaction and higher adsorption of MB molecules on the surface of sample Nb_2O_5-150. Niobium pentoxide, which was a white powder, acquired an intense blue color after the adsorption of the cationic MB dye, whose adsorption was highest for sample Nb_2O_5-150. This absorptive property may correlate with the facile N_2 adsorption on the surface area (SA) of 151 $m^2\ g^{-1}$ (Table 1S and Figure 3S, Supplementary Material), enabling good exposure of active sites that had a positive effect on photoactivity. In contrast,

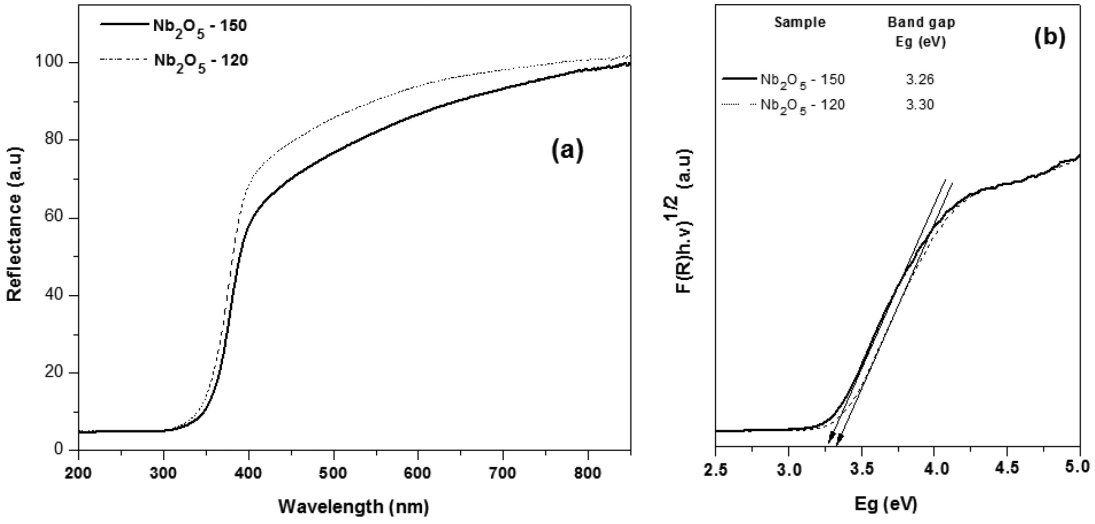

Figure 4. *(a) UV-Vis diffuse reflectance spectra (DRS) of the Nb_2O_5 samples; (b) Tauc plot for the direct allowed transition obtained from DRS data (band gap values (Eg) are also shown in the inset)*

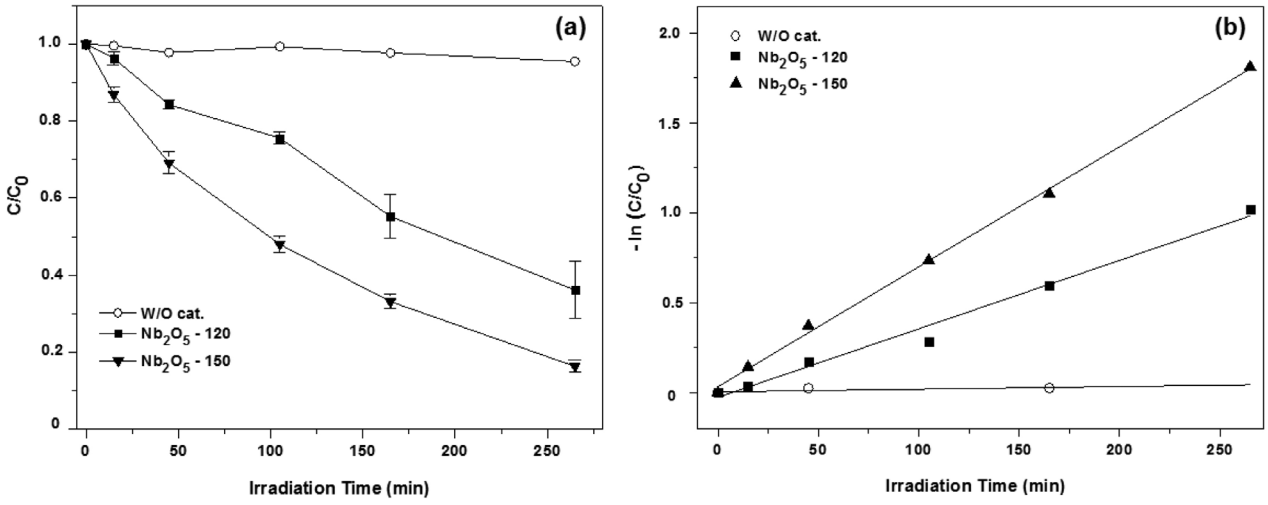

Figure 5. *(a) Photodegradation curves of methylene blue (MB) dye with synthesized Nb_2O_5 samples under UVC irradiation; (b) kinetic plots using the pseudo-first-order model*

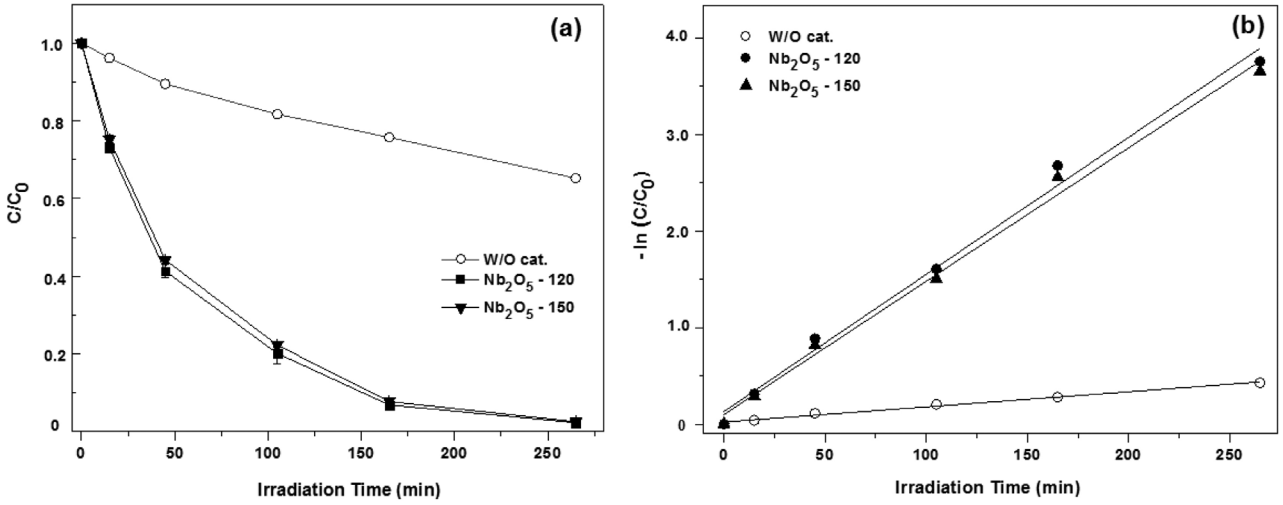

Figure 6. *(a) Photodegradation curves of indigo carmine (IC) dye with synthesized Nb_2O_5 samples under UVC irradiation; (b) kinetic plots using the pseudo-first-order model*

Table 2. Rate constants (k) and linear correlation coefficients (R^2) for the MB and IC photodegradation under UVC irradiation

Sample	k_{MB} / min^{-1}	R^2	k_{IC} / min^{-1}	R^2
Photolysis (W/O cat.)	0.0001	0.7699	0.0016	0.9905
Nb_2O_5-120	0.0038	0.9851	0.0142	0.9912
Nb_2O_5-150	0.0067	0.9985	0.0138	0.9935

W/O cat.: without catalyst.

the sample Nb_2O_5-120 presented an irregular N_2 adsorption with a poor SA value of 9 m^2 g^{-1}.

For the IC photodegradation (Figure 6a), the direct photolysis was nearly 30%, which demonstrated that IC molecules are more likely to degrade by direct photolysis under UVC irradiation than MB molecules. Also, the both synthesized Nb_2O_5 materials demonstrated excellent efficiency to remove IC dye, with approximately 100% removal efficiency (Figure 2Sb). The rate constants of the two samples were also very similar, showing values of 0.0142 and 0.0138 min^{-1} for the samples Nb_2O_5-120 and Nb_2O_5-150, respectively. Unlike the MB, no change was observed in the color of the Nb_2O_5 powders for the IC tests, indicating that the photodegradation probably takes place exclusively by radical attack on the IC molecules in solution without any adsorption. We compare the photocatalytic performance of the synthesized Nb_2O_5 samples in our present work with that of previously reported studies. The data are summarized in Tables 2S and 3S (Supplementary Material). The results from this work are superior to many others reported Nb_2O_5 catalysts for the photodegradation of dye wastewater.

It is well known that photocatalysis with semiconductors occurs in two main ways: (*i*) by the direct transfer of electrons (e^-) from adsorbed molecules on the semiconductor surface to the hole (h^+) of the photoactivated semiconductor (in this case, Nb_2O_5 samples), forming unstable radical molecules of pollutant; (*ii*) by the formation of highly reactive radicals (mostly hydroxyl radicals) on the photocatalyst surface, which act on the molecules of pollutant (in this case, MB or IC), promoting its degradation.[41,42] With this in mind, it can be concluded from the results presented here that the photocatalytic process for the MB was strongly influenced by the adsorption of their molecules. This process could be a simple adsorption (physical or chemical adsorption) or the above-cited process (*i*). On the other hand, the IC photodegradation was not affected by any adsorption, which leads us to believe that the IC degradation mainly occurred by typical photocatalysis, i.e., by the formation of highly reactive radicals (*ii*).

The possible photodegradation products of MB and IC dyes were investigated using high-performance liquid chromatography (HPLC). These results are presented in Figures 4Sa (MB) and 4Sb (IC), in Supplementary Material. Based on the results obtained by HPLC, it was possible to observe the presence of photodegradation byproducts in reactions with both dyes, MB and IC. The MB dye was identified by a peak at a retention time of 1.02 min (first peak) from the chromatogram in Figure 4Sa. After the photocatalytic process with Nb_2O_5 samples, this peak has decreased clearly in comparison with the original peak of MB without degradation. Also, the formation of byproducts was observed with the appearance of peaks at different retention times between 3.6 and 4.6 min (other peaks in Figure 4Sa). However, it is important to note that MB was not completely converted after 260 min of reaction time.

The IC dye was identified by a peak at a retention time of 1.06 min (first peak) from the chromatogram in Figure 4Sb. The IC dye, in turn, was probably completely degraded after 260 min of photodegradation. The formation of byproducts was observed with peaks in retention times between 1.4 and 1.6 min (other peaks in Figure 4Sb). Thus, the results obtained by HPLC successfully confirmed the photodegradation process for both dyes, being that the process for the IC seems to be more effective than for MB, as already indicated by its high removal efficiency observed in Figure 2S. Considering that the IC molecules did not present significant adsorption on the photocatalyst surface, it can be concluded that the adsorption process was not essential to promoting photodegradation. Taking a step further, we can say that the photodegradation process without adsorption was more effective (IC dye degradation), which demonstrates the important role of the reactive radicals for the photodegradation of organic molecules using semiconductors.[41,42]

Reduction of the free fatty acids (FFA) from waste cooking oil (WCO)

Non-catalytic photoesterification

The acid value (AV) of the waste cooking oil (WCO) was 15.8 mg KOH g^{-1}, corresponding to 7.9% of free fat acids (FFA) in the composition of WCO. The photoesterification tests were first performed without Nb_2O_5 (blank). This analysis is important since although the FFA are weak Brønsted acids, they are active catalysts for esterification, and autocatalytic activity is generally observed.[43] Figure 5S (Supplementary Material) shows the effect of UVC irradiation on the non-catalytic photoesterification in different ethanol/oil molar ratios (E/O = 20:1 and 5:1). A non-catalytic reaction with FFA conversion (C_{FFA}) of around 45% was observed using a 20:1 molar ratio. Also, the FFA conversion significantly decreased to very low values (around < 10%) using a 5:1 molar ratio. However, the use of UVC irradiation had no significant effect on the FFA conversion for both molar ratios. Thus, these results showed that the excess alcohol used (20:1 molar ratio) apparently leads to a non-catalytic reaction without interference from UVC irradiation. Excess alcohol shifts the equilibrium of the reaction towards the formation of products since it is a reversible process, as presented in the equation in Figure 6S (Supplementary Material).[12,13]

Non-catalytic esterification was reported in some works using different types of soybean oil deodorizer distillate;[43] karanja oil;[44] and sugarcane bagasse.[45] The Table 4S (Supplementary Material) summarizes these results. The main limitation observed in these studies was the high temperature employed and the high alcohol/oil molar ratio used to obtain expressive results. These limitations make the development of new and more effective catalysts an important subject of study.

Photoesterification using Nb_2O_5: effect of reaction parameters

The Figures 7a and 7b show the effect of UVC irradiation and the ethanol/oil molar ratio on the photoesterification using Nb_2O_5-150 and Nb_2O_5-120. Firstly, the FFA conversion (C_{FFA}) using the 20:1 molar ratio with the two samples of Nb_2O_5 was close to the value obtained from the non-catalytic tests (around 45%). Once again, no effect of the UVC irradiation was observed. The FFA conversion was probably mainly due to the excess alcohol (20:1 molar ratio) and not to the activity of the photocatalyst, as already discussed previously. On the other hand, the activity of the two Nb_2O_5 samples was evidenced, reducing the ethanol/oil molar ratio to 5:1. Using the both Nb_2O_5 samples, there was around a 2.5-fold increase in FFA conversion compared to the non-catalytic test without irradiation, and an increase of 6.3-fold in the FFA conversion using UVC irradiation as compared to the non-catalytic test. A similar performance of materials was observed in the tests, which is in agreement with the structural and morphological analyses. Therefore, this result shows that Nb_2O_5 samples presented photoactivity, which was explained by the increase in the FFA conversion using irradiation.

To the best of our knowledge, the photocatalytic property of the Nb_2O_5 for FFA esterification has still not been demonstrated by other studies. In this work, the Nb_2O_5-150 photocatalyst presented the best performance under UVC irradiation, obtaining a product (oil) with a 4.49% FFA concentration. However, this value is still slightly above the ideal value (less than 1.0% of FFA content) to carry out the transesterification reaction without saponification of the FFA's[46] but an increase in reaction time may favor the complete photoesterification reaction.

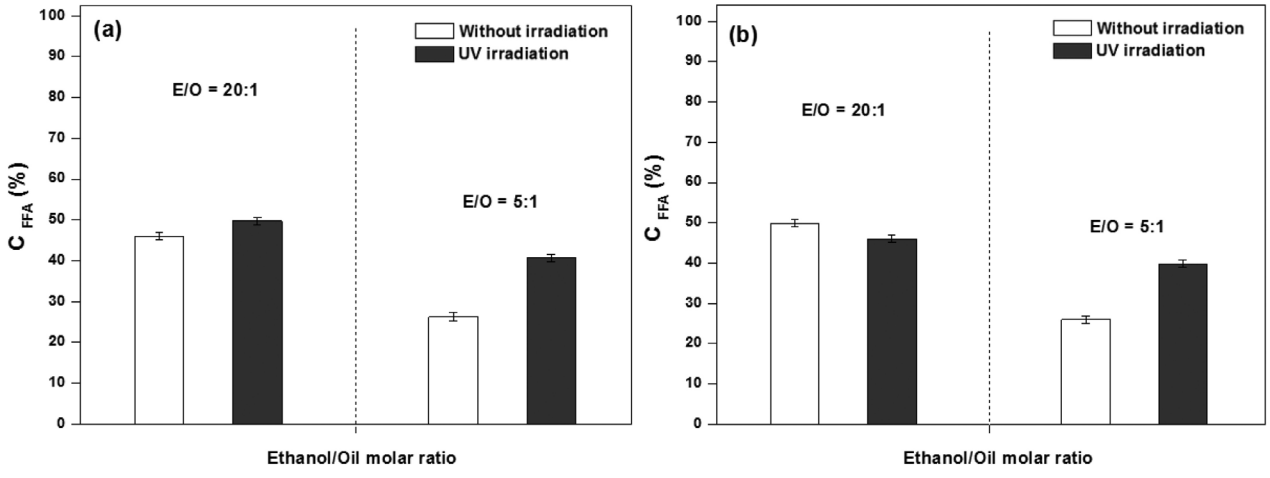

Figure 7. *Effect of UV irradiation and ethanol/oil molar ratio on the reduction of AV: (a) Nb_2O_5-150; (b) Nb_2O_5-120*

Heterogeneous acid catalysis is limited by the high temperature (above 100 °C) and high molar ratio required for optimal performance. A wide variety of materials have already been used, such as zeolites (H-BEA and Beta protonated zeolite)[46] reduced graphene oxide;[47] green copper oxide nanocatalysts;[48] sulfonated SnO_2 nanocatalysts[49] and many others. In recently studies, semiconductors materials were evaluated for esterification using: waste cooking oil,[17,28] non-edible oils,[12,13,50] oleic acid,[14] and others. The Table 5S (Supplementary Material) shows a comparison of photoesterification using these different semiconductors. An interesting point observed in our results was the use of more moderated reactions conditions (temperature, molar ratio and reaction time) than reported in others studies.

A basic mechanism of the photoesterification reaction is as follows: when a semiconductor-based heterogeneous photocatalyst is illuminated by light with photons with energy higher than its gap energy, electron-hole pairs become diffused to the surface of the photocatalyst and participate in the chemical reaction. The free electrons (e^-) and holes (h^+) have the potential to promote redox reactions of the surrounding molecules into the free radicals under UVC irradiation. An important step is the adsorption of molecules (FFA and ethanol, in this case) on the surface of the (photo) catalyst, mainly at surface sites which may act as Lewis acid sites. This step may be kinetically favored due to the vast number of acid sites. The photo-generated holes (h^+) react with ethanol (CH_3–CH_2–OH) adsorbed over the surface, producing hydrogen ions (H^+) and CH_3–CH_2–O$^\bullet$ radicals. Simultaneously, $^\bullet$HOOC–R radicals are formed by the reduction of FFA (HOOC–R) adsorbed over the surface, reacting with photogenerated electrons (e^-). Subsequently, the radicals react to form the intermediates and final products (ethyl-ester and water). Finally, the transfer of the products from the interface region to the liquid phase takes place.[13,17,51,52]

CONCLUSIONS

It was possible to conclude that, even at the lowest synthesis temperature, the Nb_2O_5 was formed by aggregate of particles with undefined morphology. The synthesized materials did not demonstrate significant optical and structure differences. On the other hand, in the photodegradation tests of the dyes under UVC radiation, the Nb_2O_5-150 sample showed higher adsorption and photoactivity than the sample Nb_2O_5-120 during the MB removal, probably because of its highest specific surface area. Therefore, the both synthesized samples presented approximately 100% of the removal efficiency for the IC dye. The HPLC results confirmed the photodegradation of both molecules (MB and IC) and also suggested the complete degradation of the IC. Under moderate conditions in the photoesterification using Nb_2O_5 (E/O = 5:1), the excess of ethanol did not affect the free-fatty acid (FFA) conversion, and it was possible to evidence the photoactivity of the synthesized samples under UVC irradiation. In this test, the photocatalytic FFA conversions using the both synthesized samples were similar and higher than the conversion in the non-catalytic reactions, indicating that these samples are promising for free-fatty acid photoesterification in vegetable oils.

SUPPLEMENTARY MATERIAL

Some images of the systems used in this work are available at http://quimicanova.sbq.org.br, as a PDF file, with free access.

ACKNOWLEDGMENTS

The authors are grateful for the CBMM (Companhia Brasileira de Metalurgia e Mineração) and the financial support of the funding agencies: FINEP (01.220381.00 and 01.13.0371.00), CNPq (408661/2021-6, 407878/2022-0) and FAPEMIG (grants number APQ-00889-18, APQ-03088-21 and APQ-00856-22). The authors wish to thank the support from LMMA sponsored by FAPEMIG APQ 00372-22; and the Coordenação de Aperfeiçoamento de Pessoal de Nível Superior (CAPES) (Finance Code 001 and 18/2020). The authors are also grateful for the support from FAPESP 2018/01258-5 and CNPq SISNANO (CNPq project No. 442575/2019-0) and INCT Programs (CNPq project No. 406925/2022-4).

REFERENCES

1. Ibhadon, A. C.; Fitzpatrick, P.; *Catalysts* **2013**, *3*, 189. [Crossref]
2. Ücker, C. L.; Riemke, F. C.; de Andrade Neto, N. F.; Santiago, A. A. G.; Siebeneichler, T. J.; Carreño, N. L.; Cava, S.; *Chem. Phys. Lett.* **2021**, *764*, 138271. [Crossref]
3. Prado, A. G.; Bolzon, L. B.; Pedroso, C. P.; Moura, A. O.; *Appl. Catal., B* **2008**, *82*, 219. [Crossref]
4. Lopes, O. F.; Paris, E. C.; Ribeiro, C.; *Appl. Catal., B* **2014**, *144*, 800. [Crossref]
5. Du, L.; Long, Z. Y.; Wen, H. M.; Ge, W. L.; Zhou, Y.; Wang, J.; *CrystEngComm* **2014**, *16*, 9096. [Crossref]
6. Shao, R.; Cao, Z.; Xiao, Y.; Dong, H.; He, W.; Gao, Y.; Liu, J.; *RSC Adv.* **2014**, *4*, 26447. [Crossref]
7. Kumari, N.; Gaurav, K.; Samdarshi, S. K.; Bhattacharyya, A. S.; Paul, S.; Rajbongshi, B.; Mohanty, K.; *Sol. Energy Mater. Sol. Cells* **2020**, *208*, 110408. [Crossref]
8. Zhang, J.; Li, D.; Qiu, J.; Wen, Z.; Luo, X.; Bian, C.; Chen, J.; Mengfei, L.; *Mater. Res.* **2020**, *7*, 115502. [Crossref]
9. Slamet, H. W. N.; Purnama, E.; Kosela, S.; Gunlazuardi, J.; *Catal. Commun.* **2005**, *6*, 313. [Crossref]
10. Sharma, Y. C.; Singh, B.; Upadhyay, S. N.; *Fuel* **2008**, *87*, 2355. [Crossref]
11. Liu, G.; Hoivik, N.; Wang, K.; Jakobsen, H.; *Sol. Energy Mater. Sol. Cells* **2012**, *105*, 53. [Crossref]
12. Corro, G.; Pal, U.; Tellez, N.; *Appl. Catal., B* **2013**, *129*, 39. [Crossref]
13. Corro, G.; Sánchez, N.; Pal, U.; Bañuelos, F.; *Waste Manage.* **2016**, *47*, 105. [Crossref]
14. Manique, M. C.; Silva, A. P.; Alves, A. K.; Bergmann, C. P.; *Mater. Sci. Eng., B* **2016**, *206*, 17. [Crossref]
15. Gao, Y.; Chen, Y.; Gu, J.; Xin, Z.; Sun, S.; *Fuel* **2019**, *236*, 1489. [Crossref]
16. Aghel, B.; Mohadesi, M.; Ansari, A.; Maleki, M.; *Renewable Energy* **2019**, *142*, 207. [Crossref]
17. Guo, M.; Jiang, W.; Chen, C.; Qu, S.; Lu, J.; Yi, W.; Ding, J.; *Energy Convers. Manage.* **2021**, *229*, 113745. [Crossref]
18. Ziolek, M.; *Catal. Today* **2003**, *78*, 47. [Crossref]
19. Furukawa, S.; Tsukio, D.; Shishido, T.; Teramura, K.; Tanaka, T.; *J. Phys. Chem.* **2012**, *116*, 12181. [Crossref]
20. Lopes, O. F.; Mendonça, V. R. D.; Silva, F. B.; Paris, E. C.; Ribeiro, C.; *Quim. Nova* **2015**, *38*, 106. [Crossref]
21. Le Viet, A.; Jose, R.; Reddy, M. V.; Chowdari, B. V. R.; Ramakrishna, S.; *J. Phys. Chem. C* **2010**, *114*, 21795. [Crossref]
22. Lazarova, K.; Vasileva, M.; Marinov, G.; Babeva, T.; *Opt. Laser Technol.* **2014**, *58*, 114. [Crossref]
23. Chen, J.; Wang, H.; Huang, G.; Zhang, Z.; Han, L.; Song, W.; Zhang, Y.; *J. Alloys Compd.* **2017**, *728*, 1928. [Crossref]
24. Bassan, I. A.; Nascimento, D. R.; San Gil, R. A.; da Silva, M. I. P.; Moreira, C. R.; Gonzalez, W. A.; Lachter, E. R.; *Fuel Process. Technol.* **2013**, *106*, 619. [Crossref]
25. Ko, E. I.; Weissman, J. G.; *Catal. Today* **1990**, *8*, 27. [Crossref]
26. Sayılkan, F.; Erdemoğlu, S.; Asiltürk, M.; Akarsu, M.; Şener, Ş.; Sayılkan, H.; Arpaç, E.; *Mater. Res. Bull.* **2006**, *41*, 2276. [Crossref]

27. Zhao, Y.; Eley, C.; Hu, J.; Foord, J. S.; Ye, L.; He, H.; Tsang, S. C. E.; *Angew. Chem.* **2012**, *124*, 3912. [Crossref]
28. Khan, M.; Farah, H.; Iqbal, N.; Noor, T.; Amjad, M. Z. B.; Bukhari, S. S. E.; *RSC Adv.* **2021**, *11*, 7575. [Crossref]
29. Murphy, A. B.; *Sol. Energy Mater. Sol. Cells* **2007**, *91*, 1326. [Crossref]
30. Zhang, Z.; Zhang, G.; He, L.; Sun, L.; Jiang, X.; Yun, Z.; *CrystEngComm* **2014**, *16*, 3478. [Crossref]
31. Oliveira, J. A.; Torres, J. A.; Gonçalves, R. V.; Ribeiro, C.; Nogueira, F. G.; Ruotolo, L. A.; *Mater. Res. Bull.* **2021**, *133*, 111073. [Crossref]
32. Qiu, J. P.; Xie, H. Q.; Wang, Y. H.; Yu, L.; Wang, F. Y.; Chen, H. S.; Lian, J. B.; *Materials* **2021**, *14*, 3783. [Crossref]
33. Falk, G.; Borlaf, M.; Bendo, T.; de Oliveira, A. P. N.; Rodrigues Neto, J. B.; Moreno, R.; *J. Am. Ceram. Soc.* **2016**, *99*, 1968. [Crossref]
34. Salim, E. T.; Ismail, R. A.; Halbos, H. T.; *Appl. Phys. A: Mater. Sci. Process.* **2020**, *126*, 891. [Crossref]
35. Ristić, M.; Popović, S.; Musić, S.; *Mater. Lett.* **2004**, *58*, 2658. [Crossref]
36. Su, T.; Zhai, Y.; Jiang, H.; Gong, H.; *J. Therm. Anal. Calorim.* **2009**, *98*, 449. [Crossref]
37. Luiz, T. M.; Nakagomi, F.; Renzetti, R. A.; Siqueira, G. O.; *Process. Appl. Ceram.* **2021**, *15*, 128. [Crossref]
38. Mai, C. T. Q.; Ng, F. T. T.; Rempel, G. L.; *Catalysis* **2018**, *30*, 176. [Crossref]
39. Zanella, D.; Bossi, E.; Gornati, R.; Bastos, C.; Faria, N.; Bernardini, G.; *Sci. Rep.* **2017**, *7*, 11413. [Crossref]
40. Mourão, H. A.; Malagutti, A. R.; Ribeiro, C.; *Appl. Catal., A* **2010**, *382*, 284. [Crossref]
41. Legrini, O.; Oliveros, E.; Braun, A. M.; *Chem. Rev.* **1993**, *93*, 671. [Crossref]
42. Hoffmann, M. R.; Martin, S. T.; Choi, W.; Bahnemann, D. W.; *Chem. Rev.* **1995**, *95*, 69. [Crossref]
43. Hussain, Z.; Kumar, R.; *Int. J. Green Energy* **2018**, *15*, 629. [Crossref]
44. Fonseca, J. M.; Cardozo-Filho, L.; Teleken, J. G.; da Silva, C.; *J. Environ. Chem. Eng.* **2018**, *6*, 4988. [Crossref]
45. Gomes, G. J.; Dal Pozzo, D. M.; Zalazar, M. F.; Costa, M. B.; Arroyo, P. A.; Bittencourt, P. R.; *Top. Catal.* **2019**, *62*, 874. [Crossref]
46. Litinas, A.; Geivanidis, S.; Faliakis, A.; Courouclis, Y.; Samaras, Z.; Keder, A.; Dmytriyuk, M.; *Biofuel Res. J.* **2020**, *7*, 1170. [Crossref]
47. dos Santos, T. C.; Santos, E. C.; Dias, J. P.; Barreto, J.; Stavale, F. L.; Ronconi, C. M.; *Fuel* **2019**, *256*, 115793. [Crossref]
48. Suresh, T.; Sivarajasekar, N.; Balasubramani, K. J. R. E.; *Renewable Energy* **2021**, *164*, 897. [Crossref]
49. Nabihah-Fauzi, N.; Asikin-Mijan, N.; Ibrahim, M. L.; Hashim, H.; Yusup, S.; Taufiq-Yap, Y. H.; Mastuli, M. S.; *RSC Adv.* **2020**, *10*, 29187. [Crossref]
50. Archana, B.; Nagaraju, G.; Yatish, K. V.; Udayabhanu, U.; Sekhar, K. B.; Kottam, N.; *International Conference on Renewable Energy Research and Education*; Andhra Pradesh, India, 2018. [Crossref]
51. Jang, Y. J.; Simer, C.; Ohm, T.; *Mater. Res. Bull.* **2006**, *41*, 67. [Crossref]
52. Liu, L.; Li, H.; Zhang, Y.; *Catal. Today* **2006**, *115*, 235. [Crossref]